https://doi.org/10.5194/egusphere-2024-3724
Preprint. Discussion started: 11 March 2025

Nationwide Application of a Rapid Tsunami Inundation Model to New Zealand: Assessing Infrastructure and Land Exposure

Tate Kimpton[1], Colin Whittaker[1], Pablo Higuera[1,2], and Liam Wotherspoon[1]

[1]Department of Civil and Environmental Engineering, The University of Auckland, New Zealand
[2]Moody's RMS, United Kingdom

Correspondence: Tate Kimpton (tkim230@aucklanduni.ac.nz)

Abstract. This study presents a comprehensive nationwide tsunami inundation assessment of New Zealand. It utilises wave amplitude data from a recent probabilistic tsunami hazard assessment (covering seven return periods at the 50th and 84th percentiles) and a computationally efficient tsunami inundation model. This modelling approach enhances the inundation accuracy of previous inundation exposure assessments, which have been limited by inconsistent and simplified inundation techniques. This study produces comprehensive nationwide inundation maps for 14 return periods along the entire New Zealand coastline. These inundation maps have been integrated with land cover and infrastructure asset data to assess New Zealand's potential exposure and identify the most vulnerable locations. The findings reveal that while commonly studied cities like Christchurch, Gisborne, and Napier are indeed highly vulnerable, significant exposure is also evident in many provincial areas such as the Buller, Westland and Thames-Coromandel Districts. In the Thames-Coromandel District, over 13,400 buildings are exposed to inundation at the 500-year return period tsunami amplitudes, representing 26.8% of the buildings in the district. Considering the land classification, the 'Low Vegetation' land cover group is the most exposed in every region, while determining the exposure of the 'Built-Up Area' is a good indicator of overall asset exposure for a region. The inundation model's efficiency, simplicity, and accuracy make it well-suited for international application, particularly in regions with similar topographic, land use, and hazard data. This versatility, combined with its speed, supports its application in further large-scale probabilistic hazard assessments and smaller, targeted scenario modelling, as well as in uncertainty analyses across diverse geographic and hazard contexts.

1 Introduction

The location of New Zealand on the Pacific Rim exposes the coastline to many potential tsunamis from local, regional, and distant sources. For example, distant source tsunamis can be triggered by earthquakes where the Nazca plate of the Pacific Ocean subducts beneath the South American plate. Due to the orientation of the plate boundaries, these tsunamis have the potential to be directed towards New Zealand, travelling uninterrupted across the Pacific Ocean with minimal energy losses (Power et al., 2021). Regionally, the southern Kermadec trench poses a tsunami threat and is a well-documented potential hazard for North Island cities (Power et al., 2021). Locally, the Hikurangi Trench and multiple local faults can not only produce large earthquakes and, therefore, tsunamis but any resulting tsunami threat is compounded by the proximity of the source and hence

https://doi.org/10.5194/egusphere-2024-3724
Preprint. Discussion started: 11 March 2025

the limited time between the earthquake and the resulting tsunami inundation (Berryman, 2005). Several other non-seismic sources have the potential to impact New Zealand, including volcanic, landslide, and bolide impacts, as listed in Berryman (2005). However, earthquakes are the most common cause of tsunamis in New Zealand based on historical records (NZPD, 2018; NZHTD, 2020). In their global review of tsunami occurrence Reid & Mooney (2023) concluded that between 1900 and 2020, 80% of tsunamis were attributed to earthquakes, 12% to landslides, 5% to volcanoes, 2% to meteorological events, and 1% to unknown causes.

Given this threat, producing accurate inundation modelling is vital to assessing exposure and risk and is integral to performing Probabilistic Tsunami Inundation Assessment (PTIA) and Probabilistic Tsunami Risk Assessment (PTRA). Probabilistic assessments consider earthquake characteristics such as location, magnitude, and slip conditions, ensuring that all relevant tsunamigenic sources are adequately represented (Williamson et al., 2020). While the tsunami hazard (shoreline amplitudes) from relevant tsunamigenic sources are well-documented in New Zealand (Downes & Stirling, 2001; Power, 2013; Power et al., 2021; Hughes et al., 2023), comprehensive inundation modelling is less well-documented; this, therefore, limits the possibility of national exposure assessments and PTRA. In New Zealand, nationwide tsunami wave amplitudes at the coastline are most recently established in the National Tsunami Hazard Model (Power et al., 2021), which documents a probabilistic assessment of tsunami wave amplitude at the shoreline. The assessment considers almost 1000 tsunami scenarios (comprising seismic events from local, regional, and distant sources). It reports the maximum shoreline amplitudes for 20 km segments of the coast for return periods between 100 and 2500 years at three percentiles (16th, 50th, and 84th). Thus, a tsunami hazard curve is attributed to each coastal segment, defining maximum tsunami amplitudes at the given return periods and percentiles.

Although advanced in understanding tsunami hazards compared to many other exposed countries, New Zealand has limited availability of current large-scale assessments of inundation and exposure. Internationally, the same trend is prevalent, with many countries having well-documented tsunami hazards (expected shoreline wave heights) but limited national inundation and exposure assessments. Tsunami hazard assessments that have been performed, such as the North-eastern Atlantic, the Mediterranean, and connected seas (NEAM) Tsunami Hazard Model (Basili et al., 2021), use amplification factors (AF) (Glimsdal et al., 2019), as an approximate method for determining the maximum inundation height, without addressing the three-dimensionality of the onshore inundation. Therefore, although it improves on Green's Law, the AF method produces estimates of maximum inundation height rather than inundation maps based on topographic conditions. Hence, its applicability in hazard assessments as an inundation modelling approach is limited by the lack of consideration for three-dimensional coastal topography, surface roughness, and the detailed inundation extents required for PTIA or exposure assessments. Similarly, in the global tsunami hazard assessment of Davies et al. (2017), inundation calculations are simplified to amplification factors (Løvholt et al., 2012). Notably, many other tsunami hazard assessments internationally do not consider inundation due to the computational cost of running hydrodynamic models at such a large scale, even with compromises to resolution. Considering the Pacific and Indian Oceans, several hazard assessments have been performed, including hazard assessments on the coastlines of Australia (Burbidge et al., 2008), Indonesia (Horspool et al., 2014), India (Roshan et al., 2016), and Canada (Leonard et al., 2014). However, as with New Zealand, the extension to high-resolution inundation maps (10 m or finer) is limited to spe-

https://doi.org/10.5194/egusphere-2024-3724
Preprint. Discussion started: 11 March 2025

cific cities and not entire coastlines. Woessner & Farahani (2020) have performed probabilistic inundation mapping of Japan's coastline using non-linear shallow water equations; however, they have had to compromise to a 50 m resolution for the inundation. Many other localised assessments exist, limited to singular cities and regions, such as Sydney, Australia (Dall'Osso et al., 2014), and Iquique, Chile (González et al., 2020). This tendency is widespread in tsunami research, where national hazard assessments and localised inundation assessments are well-documented, but large-scale inundation and exposure assessments are either absent or limited. This lack is due to time, cost, and computational constraints at the current level of efficiency and accuracy of tsunami inundation models. These models must consider coastal geomorphology, topography, and hydraulic roughness associated with differing land uses (Imamura, 2009), significantly increasing computational cost compared to the propagation stage performed in hazard models. As Behrens et al. (2021) emphasise in their review of research gaps within probabilistic tsunami hazard and risk analysis, one of the limitations associated with large-scale tsunami risk assessments, and therefore the reason for their relative absence, is the current computational cost of inundation modelling. Overcoming this limitation requires significant simplification or approximation of the inundation process, such as reducing the complexity of the model, the number of simulations, or the resolution of the meshes, resulting in uncertainty and inaccuracy of the inundation outputs. Reducing the number of inundation scenarios can be achieved by applying the source clustering approach of Williamson et al. (2020), while the utilisation of approximate models or statistics such as amplification factors (Løvholt et al., 2012; Glimsdal et al., 2019) has previously been used, as well as employing machine learning-based tsunami emulators (Sarri et al., 2012). However, these simplifications highlight the ongoing need for innovation in balancing computational feasibility with model accuracy and practicality.

Horspool et al. (2015) and Paulik et al. (2020a) have independently published national exposure assessments to tsunami, both of which used simplifications to enable their large-scale assessments of inundation. Horspool et al. (2015) performed a nationwide probabilistic assessment of building loss, fatality rates, and injury rates, coupling the offshore probabilistic tsunami hazard model with an attenuation model (based on empirically derived attenuation factors), therefore, running inundation modelling for each tsunami scenario. Another New Zealand study attempting to understand exposure to tsunami inundation is that of Paulik et al. (2020a), who use the tsunami evacuation zones of New Zealand as a proxy for inundation. They determined the population's exposure, considering land uses and multiple infrastructure classes for New Zealand evacuation zones. Some localised infrastructure research has been conducted, such as that of Williams et al. (2019), who consider a single tsunami event (indicative of a 2500-year return period) for inundation and perform an in-depth infrastructure assessment for Christchurch. However, the single-city scenario is challenging to scale up due to the lack of comprehensive nationwide inundation modelling.

Although each study enables an improved understanding of tsunami exposure, each of the described methodologies contains limitations. Horspool et al. (2015) acknowledge that the inundation determined by the attenuation modelling procedure results in crude approximations. This is due to the two-dimensional extension of the attenuation method, which does not include gravitational effects (from topographic slope variations, for example) or differences in land cover roughness (such as the difference between the energy dissipation potential of dense forest and open land); therefore, inundation attenuation fol-

https://doi.org/10.5194/egusphere-2024-3724
Preprint. Discussion started: 11 March 2025

lows a linear profile. Kimpton et al. (2024) explore this by comparing the attenuation method to Cornell Multi-grid Coupled Tsunami (COMCOT) numerical simulations in two New Zealand cities. In their case studies of Gisborne and Christchurch, New Zealand, they quantify that the attenuation method only yields a 44.3% and 58.9% F1 score, respectively, when comapred to the inundation captured by hydrodynamic numerical modelling from COMCOT. Their results confirm that the attenuation method lacks accuracy when applied to complex topography such as estuaries, rivers, and low-lying land, agreeing with Horspool et al. (2015). Additionally, some local land cover variations are disregarded since the attenuation model is based on a limited set of empirically derived rules. Therefore, the inundation extents and inundation depths used for loss modelling (property loss, fatalities, and injuries) are based on crude approximations of inundation. The Paulik et al. (2020a) approach is limited by the inconsistent methodologies and different levels of conservatism in the evacuation zone inundation modelling. Although the orange evacuation zone often indicates the 500-year return period inundation (Paulik et al., 2020a), the approaches used to determine evacuation zones differ from one region to another, with some using hydrodynamic modelling and others using attenuation methods. The amalgamation of these different evacuation zones produces a large-scale assessment; however, in addition to the aforementioned limitations in evacuation zone development, evacuation zones do not cover the entirety of New Zealand. These inconsistencies reinforce the need for national consistency.

As described, current exposure assessments in New Zealand are based on either inundation from small-scale numerical modelling, large-scale application of low-complexity attenuation modelling (that compromises substantially on accuracy for efficiency) or the amalgamation of existing inundation studies. Therefore, there is no comprehensive, high-resolution, nationally consistent inundation modelling, and any such existing exposure and risk assessments are limited by the availability and reliability of inundation estimates. In this paper, we perform consistent nationwide inundation modelling using the model developed by Kimpton et al. (2024), a two-dimensional rapid tsunami inundation model built upon the equations from Smart et al. (2015). The model utilises the Bernoulli equation and relevant approximations, such as the shallow water assumption, to simulate tsunami inundation. This approach, therefore, enables a nationally consistent assessment of exposure to land cover and critical built assets across the country.

The efficiency of the Kimpton et al. (2024) model enables the nationwide application in the current study. This takes into account maximum coastal wave amplitudes for multiple return periods across New Zealand while improving on the accuracy and scope of previous national modelling attempts. The development of nationally consistent inundation maps for New Zealand enables an improved and updated understanding of New Zealand's national exposure to tsunamis and the potential societal and asset impacts. This methodology also offers a solution to international hazard studies, offering a framework for assessing tsunami inundation and exposure nationally or at a wide regional scale.

The paper is organised as follows: first, it summarises the background of the inundation model and the required inputs to run it nationally. Next, it describes the methodology for applying the model to the national context, outlining the process of converting shoreline hazard data into comprehensive inundation maps. The paper then presents the results, integrating land

https://doi.org/10.5194/egusphere-2024-3724
Preprint. Discussion started: 11 March 2025

cover and infrastructure datasets into the inundation maps to determine exposure across the various return periods. Finally, conclusions are drawn, and recommendations for further research are provided.

2 Model Overview

In this research, the inundation model is implemented using a discrete rectangular grid (10 m by 10 m) that incorporates topographic data, initial wave amplitude, and land cover roughness variables. Kimpton et al. (2024) developed a Python code that performs inundation simulations over a specified area. The modelling equation is applied sequentially within the specified area, starting from the shoreline (which is prescribed a wave crest level), "crawling" inland and calculating inundation one cell at a time. The inundation map produced by the two-dimensional model determines the maximum inundation extent and depth rather than providing a time series of inundation. However, as an approximation, a 'level' variable produced by the code indicates the progression of inundation (Kimpton et al., 2024). Hence, although a tsunami typically manifests as a series of waves, the predicted inundation extent by the model reflects inundation from a single (i.e., the highest) wave. For further information on the model equations and methodology, the reader is referred to Kimpton et al. (2024).

The equations underpinning the model introduce certain limitations, particularly the absence of mass conservation. This limits the model's accuracy when addressing regions of significant horizontal topographic convergence or divergence (e.g., funnels or valleys). Notably, this limitation is shared among simplified inundation methods, including the commonly applied attenuation method. Additionally, encountering a steep enough negative slope may increase inundation depth; however, the overall water level relative to the datum is still reduced as the topographic decrease surpasses the inundation increase. This phenomenon is explored in detail by Kimpton et al. (2024) concerning the lee side of dune systems and the "pooling effect" that can occur. However, this pooling is justifiable and aligns with the findings of Yoshii et al. (2017), who demonstrated water accumulation on the lee side of dunes in the presence of sufficiently high tsunami wave amplitudes relative to the dune system. It is also important to note the uncertainties in modelling a dune system's changing profile and geomorphology during a tsunami event (which are out of the scope of this model), as this can further influence the inundation dynamics.

Furthermore, the proposed model does not explicitly address the transformation and interaction of flows during inundation. Rather, it advances the maximum inundation depth inland, generating inundation depths across a grid-based region. For detailed wave phenomena and instantaneous wave characteristics, three-dimensional hydrodynamic modelling is required. However, the effectiveness of such modelling is highly dependent on the spatial resolution of the input data and the accuracy of roughness classifications. Without these, low-resolution data and inaccurate bottom boundary roughness compromise the model's accuracy, making the computational cost of solving complex equations less justifiable. Despite the limitations of the current modelling method, the model proves to be an efficient and useful tool for inundation assessments, making it valuable for the large-scale applications demonstrated in this research.

https://doi.org/10.5194/egusphere-2024-3724
Preprint. Discussion started: 11 March 2025

2.1 Model Inputs

Three critical variables are required to perform the inundation and run the model for a given area: topographic data (elevation), land cover data (roughness) and shoreline wave crest level (wave amplitudes). In addition to these variables, tidal data determines the initial water level from which the wave crest is measured. In New Zealand, this is typically Mean High Water Spring (MHWS), which describes the highest level that spring tides reach, on average, over an extended period (e.g., 20 years). This is more conservative than a Mean Sea Level (MSL) approach, which averages the sea level over time without accounting for tidal variations. Although more conservative, the uncertainty surrounding tsunami wave arrival time, and therefore tidal level, justifies this approach which has been used in multiple localised case studies in New Zealand. Therefore, obtaining national MHWS data is also essential. The following subsections outline these variables and the data used to perform the nationwide analysis.

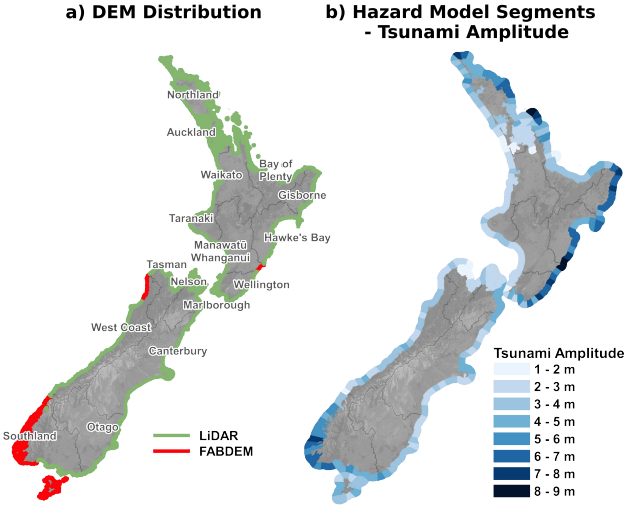

Figure 1. a) New Zealand DEM data used to represent topography in the model, separated into locations with LiDAR and FABDEM. b) New Zealand national tsunami hazard wave amplitudes for the 500-year 50p return period – separated into the 20 km coastal segments based on Power et al. (2021)

2.1.1 Topographic Data

Tsunami inundation alongside coastal flooding and sea level rise assessments require an accurate coastal digital elevation model (DEM). DEMs from multiple independent Light Detection and Ranging (LiDAR) surveys conducted over the past 20 years are obtained through Land Information New Zealand (LINZ), with resolutions up to 1 m in multiple regions (LINZ, 2023). These LiDAR datasets are merged at locations where the minor elevation variations between surveys have a minimal effect on the inundation outcomes, such as cliffs or isolated beaches. Each DEM is captured with slightly different LiDAR pulse density and vertical accuracy, with the density ranging from 1 to 16 pulses per 1 m^2 and vertical accuracy ranging between ± 0.1 to ± 0.5 m

https://doi.org/10.5194/egusphere-2024-3724
Preprint. Discussion started: 11 March 2025

at the 95% confidence interval (LINZ, 2023). In addition to the LiDAR surveys, the Forest And Buildings removed Copernicus 30 m DEM (FABDEM) data is necessary to cover additional areas not included by LiDAR surveys (Hawker et al., 2022). FABDEM addresses building and tree height biases found in the Copernicus GLO 30 Digital Elevation Model (DEM). These data are provided globally at a 1 arc-second (~30 m) grid spacing. Hawker et al. (2022) utilised machine learning techniques to remove buildings and forests from the Copernicus DEM, producing the first global elevation map with these features removed at 1 arc-second grid spacing. The regions of Manawatū-Whanganui, Southland, and West Coast are the only areas not covered by LINZ LiDAR and, therefore, require supplementary FABDEM elevation data. All other regions have comprehensive region-wide LiDAR coverage, as illustrated in Figure 1. Additionally, the Mean High-Water Spring (MHWS) tidal level is determined above the DEM datum. The MHWS is derived from primary and secondary port tidal data along the coast. The MHWS tidal level applied to the modelling considers the weighted average of multiple alongshore ports within proximity. Therefore, the shoreline is determined based on the intersection of the DEM and the MHWS tidal level, which sets the 0 m elevation as the MHWS level. A flood fill model is run from the ocean to the 0 m elevation to determine the shoreline from which the inundation starts.

2.1.2 Land Cover

Land cover specifications inform the assignment of a roughness aperture based on the land use, which is used here as a proxy for energy dissipation potential. For the New Zealand nationwide analysis, land cover classifications are defined using the Land Resource Information Systems (LRIS) Portal, which contains the New Zealand Land Cover Database (LCDB) (LRIS, 2018). The LCDB database is a multi-temporal, thematic classification of New Zealand's land cover, defining 33 mainland land cover classes. Kimpton et al. (2024) extend the roughness aperture approach of Smart et al. (2015) by calibrating the roughness apertures for the LCDB land covers to numerical modelling results that also considered roughness variation and a similar spatial resolution. Therefore, five generalised roughness values for five land cover groups were determined. By definition, as the roughness aperture increases, the energy dissipation potential decreases. This means that the most commonly defined Darcy friction factor (f) is inversely proportional to the roughness aperture, and therefore the roughness aperture is inversely proportional to energy dissipation. As a result, the roughness apertures applied to the five land cover groups, based on the analysis of Kimpton et al. (2024), were Built-Up Area: 40, Tall Vegetation: 75, Low Vegetation: 150, Bare and Urban Open: 200, and Water: 2000. Harbours have been added to the land cover classification and assigned a roughness aperture of 5000. This decision on the harbour roughness aperture was informed by the asymptotic nature of the roughness aperture. This indicates that on flatter terrains/bathymetry (such as harbours), once the roughness reaches a certain threshold, additional roughness changes result in only minor extensions of the inundation distance (Kimpton et al., 2024). However, it is justified to assign harbours a higher roughness aperture than estuaries and other water bodies due to their lack of restrictive entrances, such as river inlets, and their deeper waters. Another key application of the land cover is to enable a better classification of the shoreline. While the flood fill to MHWS method establishes the shoreline, this approach naturally includes low-lying areas, estuaries, and rivers, encompassing features like mangroves and coastal saline vegetation. Although these land covers are part of the initial water level, they often contribute to tsunami energy dissipation. To address this, the starting point for tsunami

https://doi.org/10.5194/egusphere-2024-3724
Preprint. Discussion started: 11 March 2025

inundation calculations excludes these areas and instead assigns them a roughness aperture. Finally, the common multi-wave nature of tsunamis can alter the land cover roughness index between waves by removing features or, conversely, entraining debris, thus altering the energy dissipation (Smart et al., 2015). Therefore, in the strict sense, these land cover classifications indicate the roughness index experienced by the initial tsunami wave. This is a simplification of the model, as well as advanced hydrodynamic models, which do not enable adaptive roughness characterisation between waves as damage and impacts occur to land cover elements. The same limitation applies to the elevation data, as coastal topography can change between waves, but these changes are not captured in the model.

2.1.3 Shoreline Tsunami Amplitude

Shoreline tsunami amplitudes are defined based on New Zealand's National Tsunami Hazard Model by Power et al. (2021). This model determines the probabilistic hazard from almost 1,000 tsunami scenarios and attributes hazard curves to segments of the New Zealand coastline. The coastline is divided into 252 segments, each roughly ~20 km in length. Power et al. (2021) uses a Monte-Carlo approach to generate hazard curves, accounting for both variability between events (such as changes in earthquake magnitude) and uncertainty factors (such as fault geometry). The process involves the repeated sampling of uncertain parameters to create multiple synthetic earthquake catalogues, from which tsunami heights are modelled for each coastal segment. Each sampling produces a hazard curve that correlates the maximum shoreline amplitude within the segment to the return period. Power et al. (2021) define the maximum shoreline amplitude as the 99th percentile of the tsunami maximum amplitude across all coastal points in a hazard zone, reducing the impact of localised outliers. These repeated simulations are then aggregated to create an amalgamated hazard curve for each segment, presenting the 16th, 50th, and 84th percentile curves.

Figure 1b illustrates the 500-year 50th percentile return period tsunami wave amplitude data across each segment in New Zealand, as produced by the probabilistic hazard model. The current research evaluates the inundation using the 50th and 84th percentile wave amplitudes (50p and 84p) for seven return periods (100-year, 250-year, 500-year, 1,000-year, 1,500-year, 2,000-year, and 2,500-year). Each wave amplitude, corresponding to a specific return period, is input into the inundation model and applied uniformly along the coastline of the corresponding segment. This simplification is necessary due to the limited availability of high-resolution, nationwide wave amplitude data. As a result, the amalgamated hazard curves represent the best available hazard estimates, offering a robust yet simplified approach to assessing the likely inundation extents along the New Zealand coastline.

2.2 Built Environment Assets

National built environment datasets were gathered to input into the exposure analysis. Assets were obtained from the LINZ open-source data service, which provides geospatial data for national assets (LINZ, 2023). Other assets could have been implemented; however, this assessment was limited by the availability of open-source national datasets. For the buildings, schools, airports and hospitals which have a polygon geometry type, exposure of the asset is included if any part of the polygon is exposed to inundation. Therefore, the exposure of each asset is unique, and not all assets are entirely exposed over their full geometries. School and Hospital locations and information were based on data from the NZ Ministry of Education and NZ

https://doi.org/10.5194/egusphere-2024-3724
Preprint. Discussion started: 11 March 2025

Ministry of Health (LINZ, 2023). The school data does not include early childhood centres. Building data is defined based on a two-dimensional representation of a building's roof, classified from LINZ aerial imagery through automated and manual methods, capturing structures of 10 square meters or more. For the transportation infrastructure, the assets were implemented as line geometries. Thus, in the case of roads and rail, the length of exposure is defined. Both sealed and unsealed roads are included. For bridges, if any part of the bridge is within the inundation area, it is considered exposed. Vehicle, train, foot traffic and farm bridges were all included in the assessment. The number of bridges was assessed rather than the length. Road geometry data contains additional classification based on the One Network Road Classification (ONRC) system adopted by Waka Kotahi (New Zealand Transport Agency) (NZTA, 2013). Table 1 describes the infrastructure datasets used to determine the national exposure, describing the asset geometry type and the data source.

Table 1. Outline of the infrastructure assets used in the exposure analysis, the geometry and source.

Asset Class	Subtype	Geometry	Source
Buildings			
	All buildings	Polygon	LINZ (2023)
	Schools	Polygon	LINZ (2023)
	Airports	Polygon	LINZ (2023)
	Hospitals	Polygon	LINZ (2023)
Transportation			
	Roads	Line	LINZ (2023)
	Rail	Line	LINZ (2023)
	Bridges	Line	LINZ (2023)

3 Nationwide Methodology

To process the inputs and generate consistent inundation data across New Zealand, the following methodology (the steps of which align with sub-figures in Figure 2) was implemented:

1. **Hazard Model Segments:** The coastal segments utilised for shoreline wave amplitude calculations in New Zealand's National Tsunami Hazard Model (Power et al., 2021) divided the New Zealand coast into sections for inundation. These segments have corresponding probabilistic wave amplitude information covering all the return period and percentile combinations.

2. **Bounding Box Extents:** As the model requires the inputs to be limited to a rectangular extent, the hazard model segments were converted into bounding boxes. A buffer of 5 km was applied to each segment to ensure sufficient inland coverage of potentially inundated land. The 5 km buffer also results in the overlap of adjacent segments, thus ensuring coverage of the entire area that could be influenced by the segment's inundation. Additional manual adjustments were made to

https://doi.org/10.5194/egusphere-2024-3724
Preprint. Discussion started: 11 March 2025

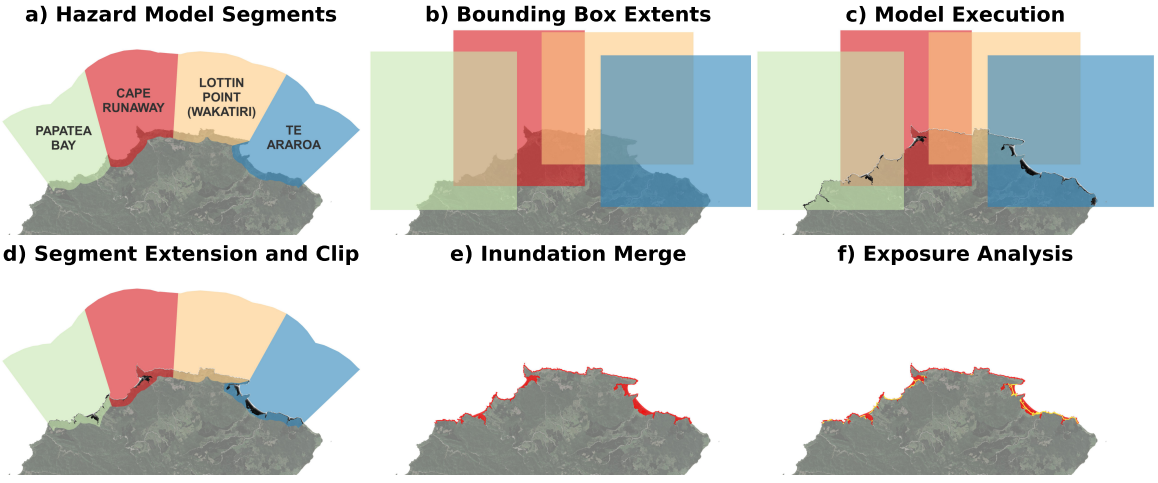

Figure 2. Methodology for running and implementing the tsunami inundation model nationwide.

some segment boundaries beyond the 5 km buffer to ensure they appropriately encapsulated coastline features, avoiding cutting off rivers, estuaries, or harbour entrances. This additional buffer resulted in a further overlap of adjacent segments.

3. **Model Execution:** The rectangular segments were used to define the extent of the DEM and Land Cover data. The inundation model was executed for each rectangular segment, computing inundation levels for each return period wave amplitude.

4. **Segment Extension and Clip:** As the modelling results of the rectangular segments had some overlap, the inundation was merged at hand-picked locations of minimal impact, such as cliffs, rather than the existing segment boundaries, which were often located at river, estuary, and harbour entrances. Therefore, the original shoreline segments were both extended inland (to accommodate the inundation associated with the largest wave amplitude elevation: 2500-year 84p wave amplitude) as well as adjacently to accommodate appropriate merging locations. This adjacent extension was done for rivers, estuaries, and harbours where the influence of these land cover types resulted in inundation beyond the original segment boundaries. The inundation associated with each return period was then clipped by the adjusted segments to obtain segment-relevant inundation that correlates to the segment's return period wave amplitude data.

5. **Inundation Merge:** Once all segments were processed for each return period scenario, the inundation data was merged into national, regional, and territorial authority inundation maps representative of the specific scenario. As some segments still resulted in overlap, as described in the previous step, the largest inundation extent and depth were retained in any such cases.

6. **Exposure Analysis:** Nationwide infrastructure datasets were integrated to assess asset exposure. This assessment involved analyzing asset exposure by region and territorial authority.

https://doi.org/10.5194/egusphere-2024-3724
Preprint. Discussion started: 11 March 2025

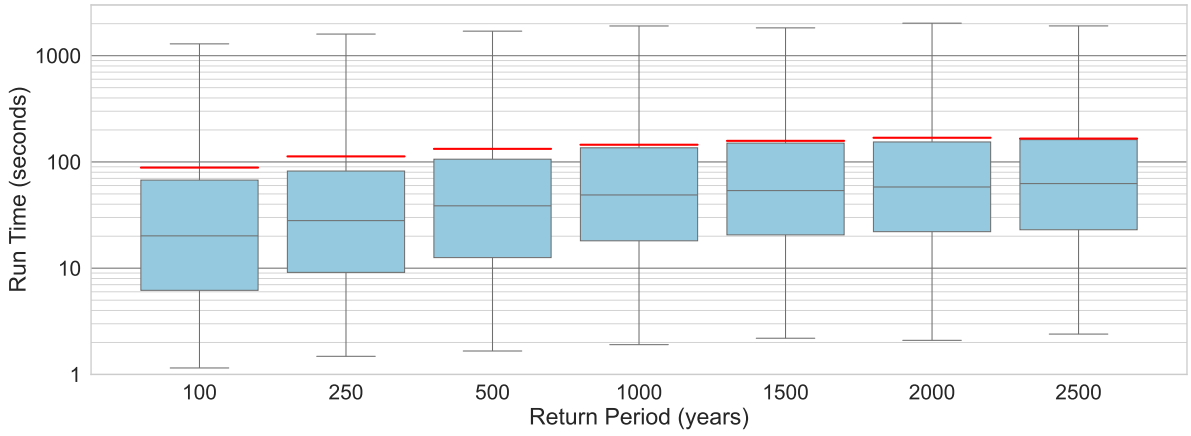

Figure 3. Box and Whisker plot showing the distribution of run times for each model segment, categorised by return period (100 to 2500 years). The plot represents runtimes for scenarios based on the 50th percentile return periods. The box shows the interquartile range (IQR) between the 25th and 75th percentiles. The red line represents the mean run time for each return period. Run times are measured in seconds and presented on a log scale.

3.1 Model Efficiency

The nationwide model ran 14 return period scenarios (7 return periods, 2 percentiles) for each of the 252 segments, totalling 3,528 simulations. This assessment was run on a standard desktop computer (using a single core per simulation) with the following specifications: PU: AMD 4700S 8-Core (3.60 GHz), RAM: 16GB. Figure 3 shows the distribution of run times (in seconds) for the tsunami inundation modelling conducted across all 252 coastal segments of the New Zealand shoreline. Each box represents the interquartile range (IQR) of run times for a specific return period and displays the median run time as a central line. The red line within each box indicates the mean run time, while the whiskers extend to show the range of run times outside the IQR. The mean runtime for the 2500-year 50p return period (largest inundation extents) was less than 3 minutes (red bar represented in Figure 3), while the median was less than 1 minute 20 seconds in all return periods. The median was far less than the mean for all return periods, indicating a significant skew towards shorter run times in the most common cases. Only a few examples resulted in larger run times; these examples are segments that encapsulate entire estuaries, harbours or sounds. Examples include the Marlborough Sounds, Kaipara Harbour, Tauranga Harbour and Dusky Sound. Overall, the total runtime for simulating all 14 return period scenarios across the entire New Zealand coastline was 147 core-hours.

https://doi.org/10.5194/egusphere-2024-3724
Preprint. Discussion started: 11 March 2025

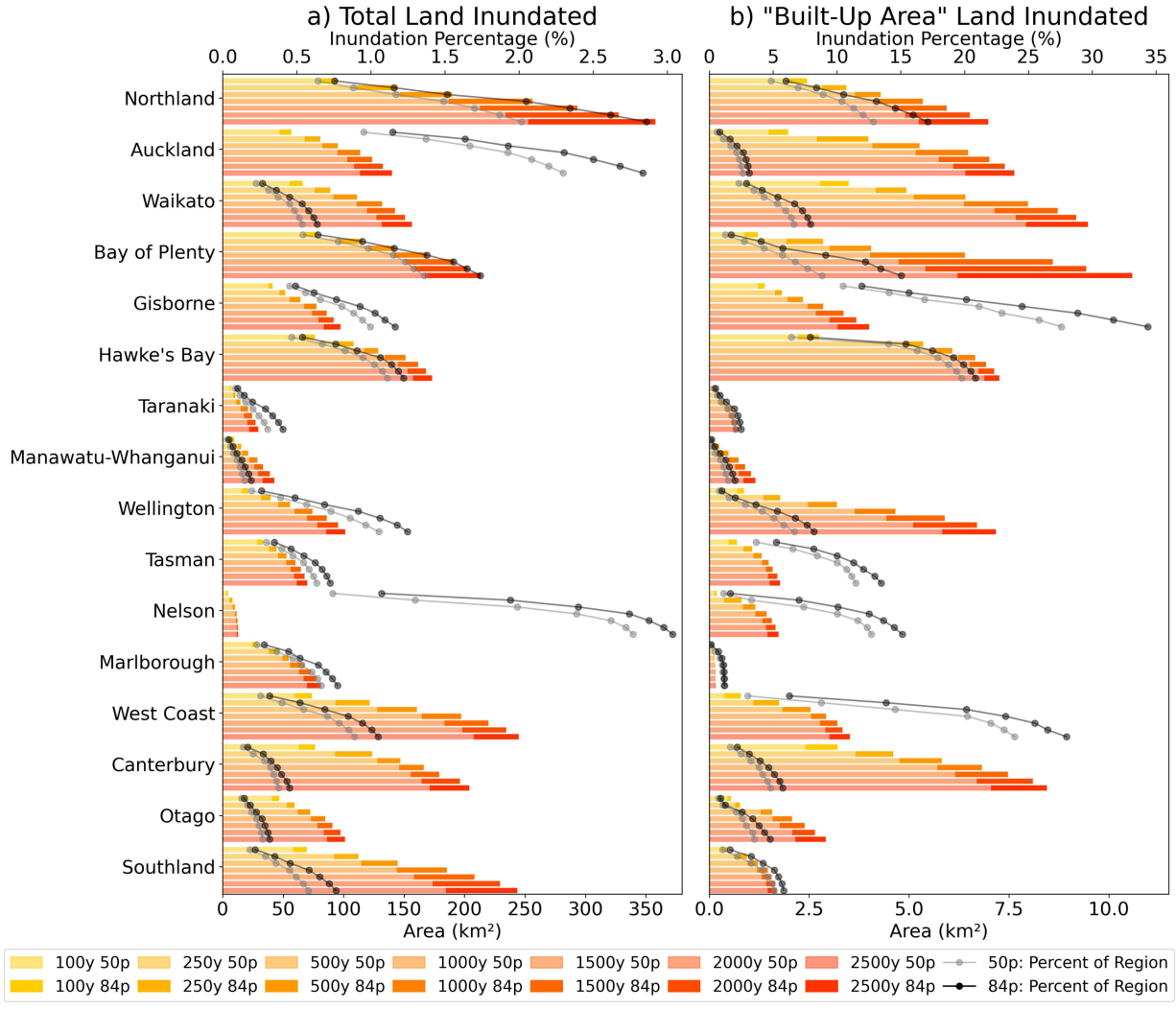

Figure 4. a) Stacked bar plot showing the absolute inundated area for each region in New Zealand, categorised by return period. b) Stacked bar plot showing the inundation on 'Built-Up Area' within each region in New Zealand, categorised by return period. Regions are plotted north to south on the vertical axis. Each subplot depicts 7 return periods (bars) for each region. Both the 50p and 84p are displayed on the same bar, 84p as the darker stacked addition. The grey and black lines (points) indicate the percentage in the plot a) this is percent of the total land $\left(\frac{\text{region\_inundated\_area}}{\text{total\_region\_area}}\right)$, and in plot b) as a percent of the total 'Built-Up Area' land $\left(\frac{\text{region\_'Built-Up Area'\_inundated}}{\text{'Built-Up Area'\_within\_region}}\right)$. The Lower horizontal axis shows the total land area inundated in the region for a certain return period in terms of km^2. The upper horizontal axis refers to the percentage of the total land area that is inundated within the region, identified by the lines and points.

https://doi.org/10.5194/egusphere-2024-3724
Preprint. Discussion started: 11 March 2025

4 Results

4.1 Inundation Extent

The first analysis considers inundation exposure to land, broken down by region, as regional councils are responsible for implementing natural hazard mitigation measures and planning. As with most flood-related hazards, the primary determinant of potential damage or loss is whether assets are located within the inundation zone. Therefore, a logical starting point is to report the land area inundated by various tsunami return period wave amplitudes. From this, the inundation is then broken down by different land cover types to determine which are most affected across the return periods. Among the various land covers, 'Built-up Area' is considered the most important, as it directly indicates exposure to population centres and built assets. Inundation for each region is presented as both the absolute area of land inundated and the percentage of the region impacted for each return period. It is important to note that while this land area has potential exposure within the specified return period, it may not all be inundated by a single event (which will have specific conditions). Therefore, the reporting of land area exposure represents the exposure potential over the entirety of the return period, whether from a single event or multiple events within the return period.

Figure 4 depicts both the absolute inundation within the region and the inundation area as a percent of the total area of the region. It displays all 16 regions in New Zealand for each return period. Each region has seven bars representing the return periods (depicted by the orange colour scheme); the 50p and the 84p are plotted on the same bar, with the darker addition to the bar representing the additional area covered by the 84p inundation. These bars correspond to the bottom horizontal axis, which displays the absolute inundation in km^2. The grey lines in Figure 4 depict the inundation as a percent of the region's total land area, with light grey implemented for the 50p and dark grey for the 84p. These percentage plots refer to the top horizontal axis. In all regions and tsunami scenarios, the percentage of the total region inundated is less than 3.5%. Considering the absolute inundated area by region, Northland experiences the greatest inundation for every return period. Figure 4a indicates that the maximum inundation for the 2500-year 50p return period in Northland is 250 km^2, inundating ~2% of the total area of the region. Nelson is an interesting case, where the absolute inundation (km^2) is the smallest for every return period (expected with Nelson having the smallest coastline); however, the proportion of land inundated within the Nelson region is relatively high. Nelson records an inundation extent of 11.7 km^2 for the 2500-year 50p return period, equating to 2.8% of the total area of the region. Taranaki and Manawatū-Whanganui have very little inundation, both in absolute terms and as a percentage of their land cover.

A useful proxy for understanding relative inundation (inundation as a percentage of the total regional area) is the geography of the region, particularly the percentage of land located within 2 km of the coastline. For example, Nelson has 27% of its land within 2 km of the MHWS shoreline, while Auckland and Northland have 47% and 26%, respectively. This high proportional proximity to the coast explains why these regions experience a higher relative inundation during a tsunami, as seen in Figure 4a. Conversely, regions such as Otago and Manawatū-Whanganui, where only 2.3% and 1.4% of the land lies within 2 km of the shoreline, show significantly lower relative inundation percentages. Regardless, the total (absolute) extent of inundation for

https://doi.org/10.5194/egusphere-2024-3724
Preprint. Discussion started: 11 March 2025

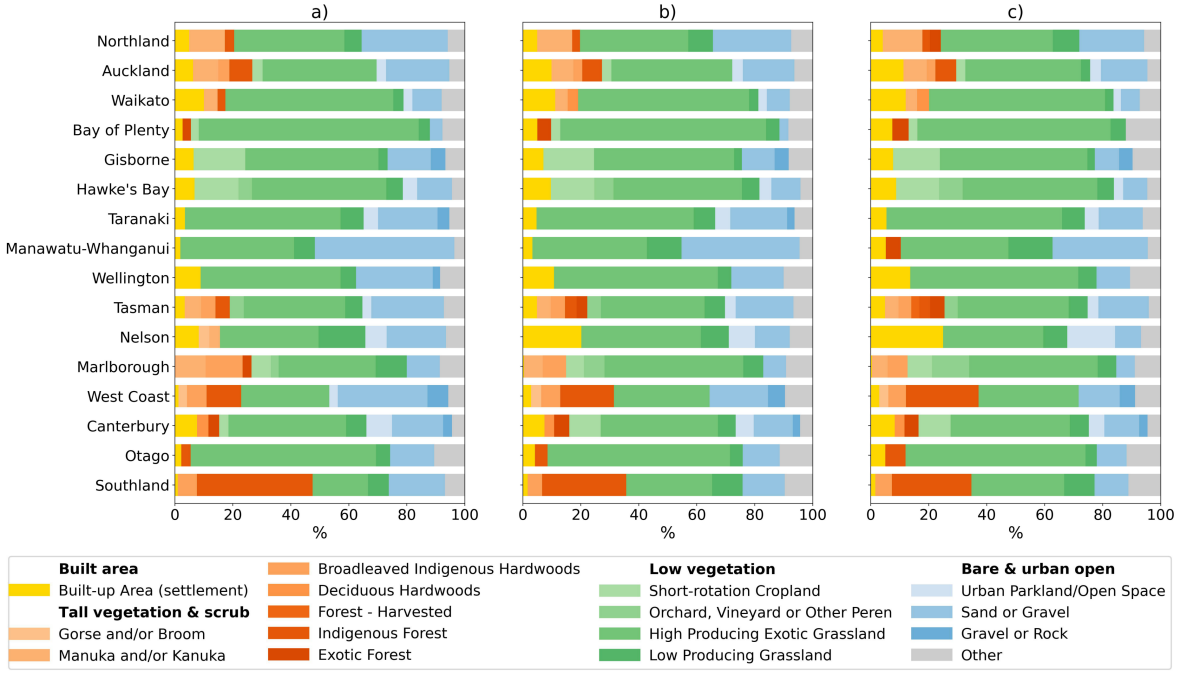

Figure 5. Stacked percentage plot determines the relative proportion of the land cover classifications within the inundation of each region. a) assesses the 100-year 50p return period, b) 500-year 50p return period, and c) 2500-year 50p return period. The different colour scales separate the land covers into the respective groups. Headings have been used in the figure legend and are represented in bold. Yellow: Built-Up Area, Oranges: Tall Vegetation & Scrub, Greens: Low Vegetation, Blues: Bare & Urban Open.

each region is important to quantify, as it gives the initial approximation of the significance of the tsunami impact to a region. However, the percentage of the region exposed gives the relative consequences faced by each region.

Assessing the 'Built-Up Area' further reveals the regions that face the most critical exposure. 'Built-Up Area' is a land cover group under the LCDB, which encompasses commercial, industrial or residential buildings, including associated infrastructure and amenities (LRIS, 2018). Therefore, the 'Built-Up Area' is the most critical land cover when considering the impact on New Zealand's cities and towns. Figure 4b illustrates the exposure of 'Built-Up Area', first by determining the total area classified as 'Built-Up Area' that is inundated for each region and return period, then as a percentage of the total 'Built-Up Area' in each region. The first observation is the significantly higher relative inundation percentages within 'Built-Up Area'. This is best observed with the tenfold increase of percentages in Figure 4b to 35%. This is likely attributed to the fact that 'Built-Up Areas' in New Zealand are predominantly located on coastlines, harbours, estuaries, and rivers rather than inland. This shows that due to the higher density of 'Built-Up Areas' on the coastline, the resulting tsunami inundation on 'Built-Up Areas' is disproportionate compared to the relative inundation of other land cover types. The most notable case is Gisborne, which does

https://doi.org/10.5194/egusphere-2024-3724
Preprint. Discussion started: 11 March 2025

not record significant absolute inundation (Figure 4a) compared to other regions. However, when determined as a percentage of its total regional 'Built-Up Area' (Figure 4b), the consequences of even relatively small amounts of inundation become far more severe. Gisborne records 27.5% of the 'Built-Up Area' being inundated in the 2500-year 50p return period - a significant proportion of the 'Built-Up Area' within the region. Taranaki, Manawatū-Whanganui, and Marlborough all remain low in terms of 'Built-Up Area' exposure, with consistently low 'Built-Up Area' inundation extents and percentages. Marlborough and Southland record relatively low inundation in 'Built-Up Area' compared to the absolute inundation of Figure 4a.

Extending the assessment to determine the effect of inundation on all land cover classifications under the LCDB provides a holistic view of the exposure. Relating inundation to independent land cover classifications clarifies the relative impact on each region. Therefore, Figure 5 illustrates the relative proportion of the land cover classifications within the inundation. Four land cover groups are evaluated: 'Built-Up Area,' 'Tall Vegetation and Scrub,' 'Low Vegetation,' and 'Bare and Urban Open.' As defined by Kimpton et al. (2024), these groups categorise the land covers from the LCDB (LRIS, 2018) into land covers with similar energy dissipation potential. For the specific land cover allocations of each group, refer to Kimpton et al. (2024); however, Figure 5 does depict some of these land covers and their corresponding groups. Figure 5 differentiates the land covers and land cover groups for the 100, 500, and 2500-year return periods. The four groups are depicted using four different colour spectrums. An additional "Other" category in each region represents the aggregation of all land covers with less than 2.5% inundation coverage.

Figure 5 immediately reveals the significant prevalence of "Low Vegetation" within the inundation extents. In every region and at the return periods considered, "Low Vegetation" is the most exposed land cover, with the only exception of Southland at the 100-year 50p return period. 'High Producing Exotic Grassland' frequently occurs as the land cover with the highest percentage of inundation. 'High Producing Exotic Grassland' is attributed to land with *'good pastoral quality and vigour reflecting relatively high soil fertility and intensive grazing management'* as described by LRIS (2018); therefore farming land is often attributed to this classification. Southland records the largest percent of its inundation impacting 'Tall Vegetation & Scrub'. While Nelson records the highest percent of its inundation impacting 'Built-Up Area'. In Manawatū-Whanganui 'Bare & Urban Open' and notably 'Sand or Gravel' contributes to a high percent of the inundation, likely due to the small hazard and expected tsunami wave amplitudes (Figure 1b), but also the extensive dune systems lining the coast. The percent of inundation in the 'Built-Up Area' is especially important to note, and as mentioned, this is generally the inundation with the highest consequence for the community. In most cases, the exposure of 'Built-Up Areas' remains constant relative to other land covers as the return period increases. However, in Nelson, a significant increase is observed, highlighting how tsunami inundation can also disproportionately affect the 'Built-Up Area' as the return period increases due to the location of the 'Built-up Area' in low-lying coastal locations. During the 100-year 50p return period, the 'Built-Up Area' area constitutes only 8.3% of the absolute inundation. However, this proportion increases significantly to 25% in the 2500-year 50p return period. This indicates that in Nelson, the impact of tsunami inundation on 'Built-Up Area' areas becomes significantly more pronounced as the return period increases. Increases in 'Built-Up Area' exposure, as a relative proportion of the land cover classifications

https://doi.org/10.5194/egusphere-2024-3724
Preprint. Discussion started: 11 March 2025

within the inundation zone, are also observed in Auckland, Wellington, Bay of Plenty, and Manawatū-Whanganui as the return period increases. This reinforces the heightened impact on 'Built-Up Areas' due to the disproportionate location of communities near coastlines in New Zealand. The inundation of other land covers presented in Figure 5, such as 'Short-Rotation Cropland', 'Orchard, Vineyard or Other Perennial Crop', 'Urban Parkland Open Space', also leads to consequential effects for the population. Inundation of production land can result in decreased food production. The inundation of "Urban Parkland Open Space" (parks, playing fields, public gardens, cemeteries, golf courses) can not only lead to disruption to areas of social importance but can also increase population risk as these are areas where people, who may not necessarily be local, congregate. As a result, it is crucial that these areas also consider evacuation measures to ensure public safety in the event of a tsunami.

4.2 Infrastructure Analysis

The consequences of tsunami events can be further explored by assessing their impact on critical built assets. Buildings, roads, and rail tracks have all been evaluated nationally across different return periods. While the assessment utilises high-resolution inundation data (10m resolution) from the model and achieves a high level of accuracy, uncertainties inherent to large-scale assessments (both continued from the probabilistic hazard modelling and from this inundation modelling analysis) require a degree of rounding. Infrastructure exposure is therefore reported to the nearest 250 buildings and the nearest kilometre for roads and rail. This approach ensures that overall trends are maintained without presenting detail that exceeds certainty. Figure 6 illustrates the exposure of these assets through a hexagon density map for the 100-year 50p, 500-year 50p, and 2500-year 50p events. The hexagons used have a side length of approximately 17.32 km. While a finer hexagon resolution could be implemented for more localised analysis, the larger hexagons were used to best capture national-level exposure. A logarithmic scale in the colour scheme bins accounts for the variations in exposure while highlighting the most vulnerable locations. It is important to note that while assets within the hexagons have the potential to become exposed within the specified return period, they may not all be inundated in a single event. In Figure 6a and Figure 6b, the roads and rail scale show a density group between 0 and 1; this is due to rounding of the logarithmic scale. All hexagons within this group have asset exposure (> 0), while the areas that have no exposure remain bare.

For building assets, during a 100-year 50p return period (Figure 6a), the hexagon encompassing Christchurch shows the highest exposure, with approximately 6,500 buildings in the inundated area. The Napier and Whitianga hexagons closely follow, with around 4,500 and 3,750 buildings affected, respectively. As the return period increases to 500-year 50p (Figure 6b), the Christchurch and Napier hexagons remain the most exposed and are the only hexagons to exceed the 10,000-building threshold, with 11,750 and 11,000 buildings inundated, respectively. The hexagon encompassing Napier notably escalates between the 100 and 500-year 50p return periods, with an almost 300% increase in the number of buildings within the hexagon extent. The Whitianga hexagon is the next highest for the 500-year 50p return period, with 5,750 buildings exposed. In the 2500-year 50p return period (Figure 6c), the Christchurch and Napier hexagons remain the most exposed, with 15,500 and

https://doi.org/10.5194/egusphere-2024-3724
Preprint. Discussion started: 11 March 2025

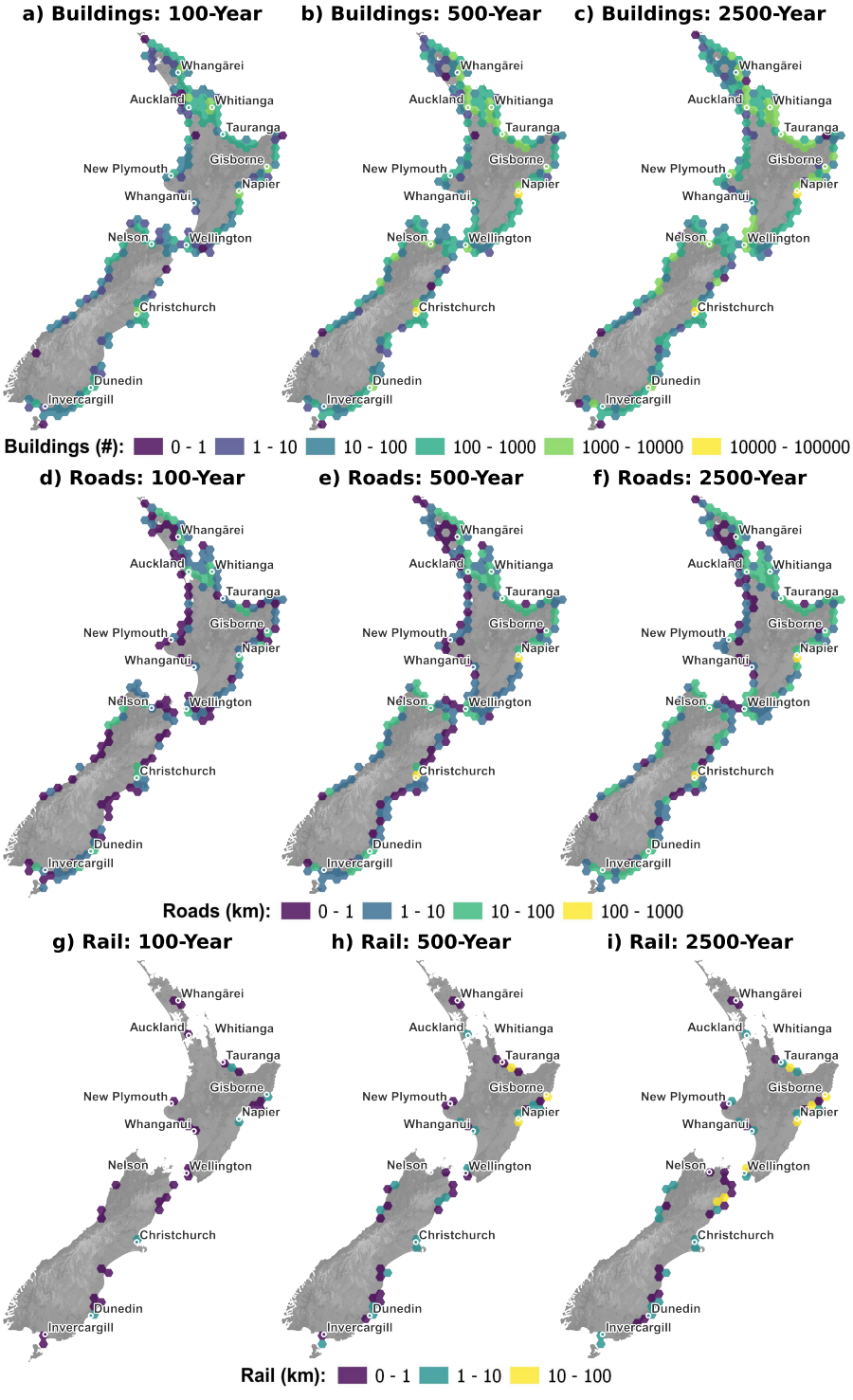

Figure 6. Hexagon Density Heatmaps represent the asset exposure for the 100-year 50p, 500-year 50p and 2500-year 50p return periods for buildings (number), roads (km) and rail (km). All scales of the heat map bins are logarithmic.

https://doi.org/10.5194/egusphere-2024-3724
Preprint. Discussion started: 11 March 2025

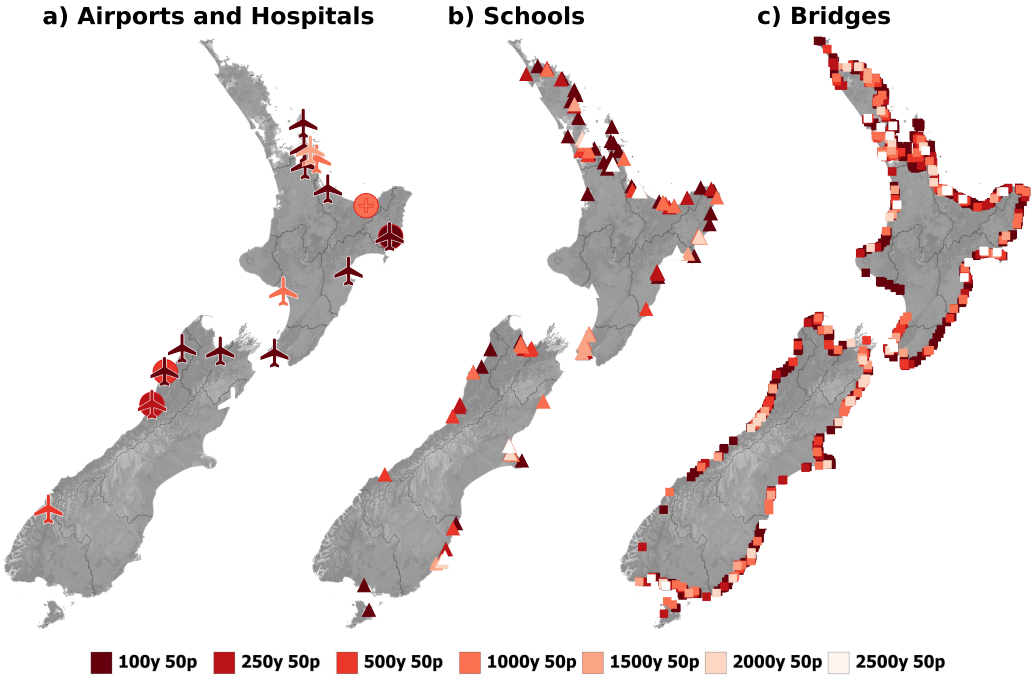

Figure 7. Asset exposure for the 50th percentile (50p) return period. The scale indicates the exposure based on the lowest return period that inundates the asset. Dark red indicates it becomes exposed as early as the 100-year 50p return period, and light red indicates that it is not till the 2500-year 50p return period that the asset becomes exposed. a) Exposed Airports and Hospitals, b) Exposed Schools, c) Exposed Bridges.

12,500 buildings exposed, respectively, and the Whitianga hexagon the next most at 7,250.

Road asset exposure demonstrates similar trends, with the Christchurch and Napier hexagons showing the greatest exposure, with approximately 85 km and 70 km of road inundated, respectively, in the 100-year 50p return period (Figure 6d). For the 500-year 50p return period (Figure 6e), the Napier and Christchurch hexagons exceed 100 km of road exposure, with 160 km and 130 km exposed to tsunami inundation, respectively. Again, the Napier hexagon sees a significant increase in exposure between the 100 and the 500-year 50p return periods, with a 230% increase to 160 km (the most exposed of all hexagons).

In addition, rail is assessed as another critical infrastructure asset for freight transport. In the 100-year 50p return period (Figure 6g), there is a much larger isolation of exposure. The Napier and Gisborne hexagons are the most exposed, each with 9 km of rail prone to inundation. Similar areas remain the most exposed as the return period increases to the 500-year return period (Figure 6h). The increase to a 2500-year return period reveals Napier, Gisborne, and Northern Kaikōura hexagons as the most exposed, with 27 km, 20 km, and 14 km of rail exposed, respectively (Figure 6i). The Kaikōura coast also becomes a hotspot for rail inundation, an important trend to note given the 2016 Kaikōura earthquake that saw disruptions to the rail line,

https://doi.org/10.5194/egusphere-2024-3724
Preprint. Discussion started: 11 March 2025

resulting in significant rail freight disruptions (Mason & Brabhaharan, 2021).

An assessment of additional key infrastructure, including airports, hospitals, schools, and bridges (vehicle, rail and pedestrian), was conducted to evaluate their exposure, given their essential roles in disaster response and community resilience. Again, due to uncertainties involved with such large-scale modelling, rounding of data has occurred to ensure overall trends are maintained without exceeding the level of certainty. Figure 7 illustrates all the assets exposed across the 50th percentile return periods. Figure 7a shows the location of the sixteen airports across New Zealand that are exposed to inundation within the airport bounds. Ten of these airports experience inundation occurring as early as the 100-year 50p return period. Wellington Airport is the only international airport exposed, with inundation at the 100-year 50p return period. Eleven airports that have scheduled passenger services on commercial airlines are inundated out of the sixteen, of which eight are inundated as early as the 100-year 50p return period. Figure 7a also shows the exposure of hospitals. Four hospital facilities have potential exposure to tsunami in NZ, two NGO (Non-Government Organisation) facilities and two public hospitals.

Figure 7b shows the school exposure to tsunami, of which just under 180 schools become exposed to the tsunami return periods considered. This exposure is determined depending on whether any part of the school outline is within the inundation bounds. Notably, schools whose boundaries extend to the top of cliffs are considered exposed if the sea below is inundated due to the resolution of the model. Sixty schools become exposed at the 100-year 50p return period. Around 68% (73 of 108 schools) of the schools exposed to and before the 500-year 50p return period have student counts of over 100 pupils.

Bridges have been assessed in Figure 7c, with nearly 1,500 expected to experience inundation within the streams, rivers, or harbours in which they are situated. Given bridges role as critical links in the transport network, the exposure is especially important due to the preferential propagation of tsunamis up rivers. Sixty-five percent of these bridges experience inundation in their waterway at the 100-year 50p return period. Bridges are also further analysed in Figure 8c, which refines the bridge analysis and shows bridge exposure by territorial authority. As bridges are located over streams, rivers, or harbours, bridge exposure may be better correlated to the level of inundation and whether it reaches the deck level (Xu et al., 2021; Tang et al., 2022). Although other failure modes may entail scour around the bridge piles. Both analyses are beyond the scope of this paper.

4.2.1 Territorial Authorities

Infrastructure and built assets in New Zealand are primarily managed at the territorial authority level (i.e., city and district councils). Out of 67 territorial authorities, 51 have coastlines susceptible to tsunamis. Figure 8 highlights the 15 most exposed territorial authorities based on the exposure of buildings, roads, and bridges. The most exposed territorial authorities are identified by ranking them across two categories (for each asset class): their 2500-year 50p return period absolute exposure and their percent exposure. The mean ranking is then calculated for each asset class and summed across asset classes to determine the most exposed territorial authorities around the country. Figure 8 captures the 15 most exposed territorial authorities and plots

https://doi.org/10.5194/egusphere-2024-3724
Preprint. Discussion started: 11 March 2025

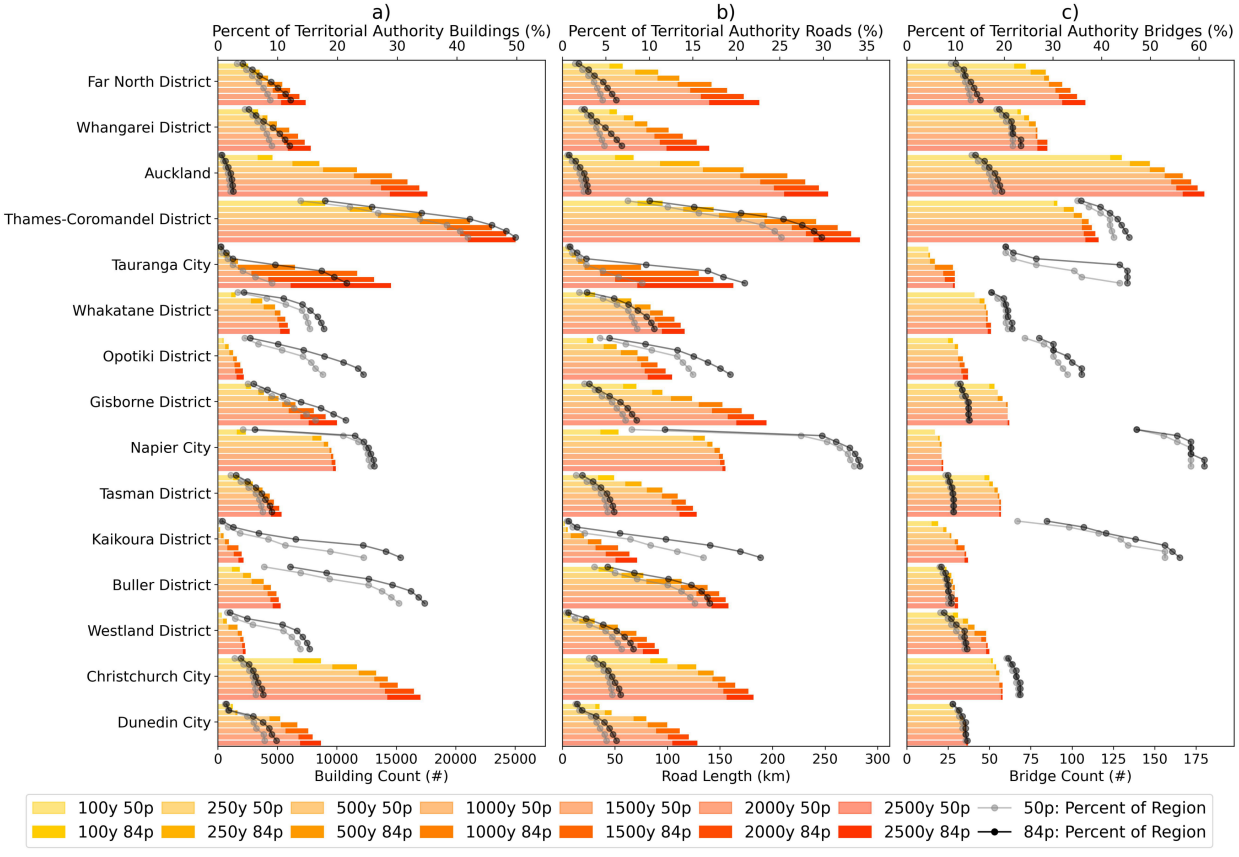

Figure 8. 15 most exposed territorial authorities based on major infrastructure exposure. Territorial authorities are ordered from north to south. a) Assesses the infrastructure exposure of buildings, b) Assesses the infrastructure exposure of roads, and c) Assesses the infrastructure exposure of bridges. The top horizontal axis in all subplots represents the percentage of the territorial authority's total asset inventory exposed for that asset, and the bottom horizontal axis in all subplots represents the total count or length of the asset exposed within that territorial authority.

the exposure of each asset class. Each plot in Figure 8 examines the total exposure in absolute terms and as a percentage of the territorial authorities' total asset inventory.

Figure 8 reveals three representative exposure conditions within the territorial authorities: 1) the absolute exposure is large relative to the percent of the total asset inventory (e.g., Auckland), 2) the absolute exposure is similar relative to the percent of total asset inventory (e.g., Thames-Coromandel District), 3) the absolute exposure is small relative to the percent of total asset inventory (e.g., Napier City, Kaikōura District). Each of these scenarios presents different challenges to the territorial authority. Regardless, across each asset class, the Thames-Coromandel District is highly susceptible in terms of total exposure and as

https://doi.org/10.5194/egusphere-2024-3724
Preprint. Discussion started: 11 March 2025

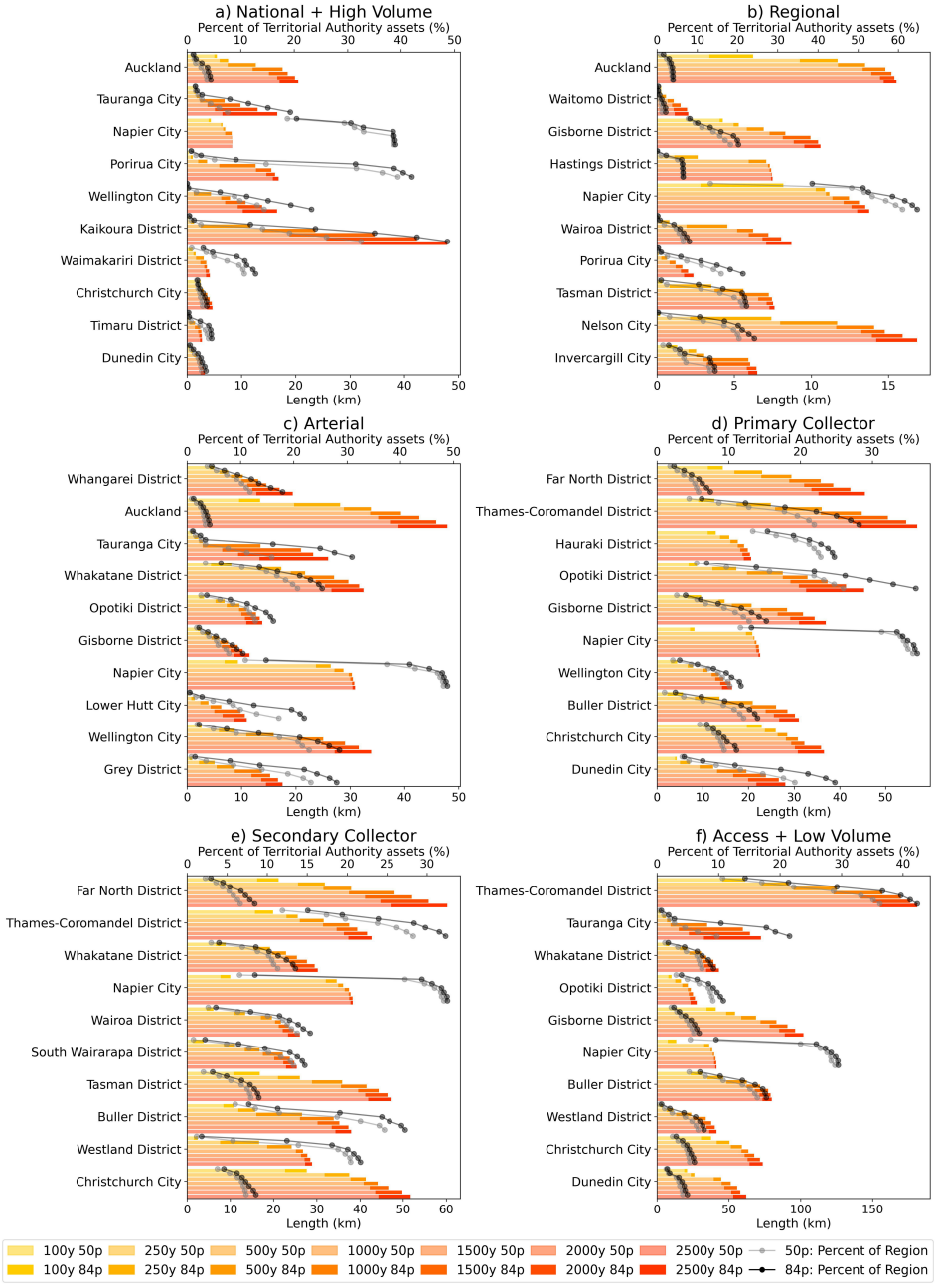

Figure 9. The ten most exposed territorial authorities for the One Network Road Classification (ONRC) road classifications. Seven scenarios are shown for each territorial authority at the 50p and 84p plotted on the same bar, 84p as an extension (darker colour) to the 50p. The bottom horizontal axis displays the total length of the road (km) inundated, while the top horizontal axis shows the percentage of the territorial authorities' total assets that are inundated. a) National and High-Volume roads, b) Regional Roads, c) Arterial Roads, d) Primary Collector roads, e) Secondary Collector Roads, and f) Access and Low-Volume Roads. Each is classified based on variables such as average daily traffic, heavy commercial vehicle daily flows, and the connectivity of populations and freight routes.

https://doi.org/10.5194/egusphere-2024-3724
Preprint. Discussion started: 11 March 2025

a percentage of total assets. It is the most exposed in terms of buildings and roads and second in terms of bridges. Kaikōura is another interesting case, with the relative exposure considerably higher than the total exposure. Napier City, as expressed earlier with the hexagon density plots (Figure 6), experiences a rapid increase in exposure early, after which exposure plateaus. This trend is likely due to the topography and the bounds which define the territory.

To assess road exposure around New Zealand, road assets can be categorised according to the One Network Road Classification (ONRC) system adopted by Waka Kotahi (New Zealand Transport Agency) (NZTA, 2013). This classification system divides the road network based on several key factors, including average daily traffic, heavy commercial vehicle daily flows, and the connectivity of populations and freight routes. Figure 9 illustrates the exposure of the road network, grouped by the ONRC classifications. Six subplots are presented, each depicting a different ONRC classification and the ten most exposed territorial authorities for that ONRC classification. Each plot should be viewed in isolation as the territorial authorities do not align between subplots; however, the north-to-south ordering of authorities is maintained. Figure 9a presents the national and high-volume roads, representing the top ONRC classification (roads with the highest daily use), while Figure 9f shows access and low-volume roads, representing the lowest ONRC classification (roads with the least daily use).

Four territorial authorities emerge as significantly exposed in Figure 9a: Napier City, Porirua City, Wellington City, and Kaikōura District. In Napier City, the exposure of national and high-volume roads is significant, with 17% of such roads affected in a 100-year 50p return period, escalating to 39% in a 2500-year 50p return period. Despite this high percentage, the total length of exposed roads remains relatively low, increasing from 4 km in the 100-year 50p return period to 8.2 km in the 2500-year 50p return period. In contrast, Kaikōura District experiences a significant increase in road exposure, from just 0.3% in the 100-year 50p return period to 32% in the 2500-year 50p return period, while having the highest absolute exposure. For regional roads, Napier City sees significant exposure in terms of the absolute exposure, but more significantly as the relative exposure where at the 500-year 50p return period, over 50% of the regional roads within the Napier City territorial authority limits are exposed. Napier City has a high relative exposure in every road classification compared to its total exposure, as well as still retaining the rapid increase to high exposure, after which the rate of increase slows down (as seen with the buildings and bridges). As the classification importance level decreases, more provincial areas of the country that are exposed are revealed, with Far North District and Thames-Coromandel District having increased total and relative exposure, emphasising their provincial nature compared to the major cities with higher road classifications. This is further emphasised in Figure 9e and 9f, which indicate Buller District and West Land District (West Coast Region) as some of the most exposed for the lower classification roads. Even though the tsunami wave amplitude (hazard) at the coast is smaller relative to other regions, the inundation results in significant exposure of assets. The considerable exposure observed in the Thames-Coromandel District, along with the broader Waikato region, highlights the need for comprehensive nationwide inundation maps and assessments. The evaluation by Paulik et al. (2020a), which relied on evacuation zones, may have underrepresented the actual exposure in some regions due to the absence of full-coverage evacuation zones.

https://doi.org/10.5194/egusphere-2024-3724
Preprint. Discussion started: 11 March 2025

5 Discussion

The assessment of inundation on land cover establishes that the 'Built-Up Area' is the most critical area to consider. Although the total land inundated gives a holistic understanding of exposure, refining the inundation to that which affects the 'Built-Up Area' is critical in determining the most consequential locations. Although some regions register significant inundation, such as Southland, the inundation to 'Built-Up Areas' remains low. In other cases, although the absolute inundation is small, the exposure of 'Built-Up Area' is high, such as Gisborne. Additionally, the variation of the inundation across different land classifications is important to understanding the exposure. By distinguishing the land cover that is affected by inundation, the exposure of other areas can be better understood. Although 'Built-Up Areas' should be used as the first instance to correlate tsunami inundation effects, other areas such as 'Short-Rotation Cropland,' 'Orchard, Vineyard or Other Perennial Crop,' 'Urban Parkland Open Space' can have lasting societal and production effects. Thoroughly examining the inundation across many land covers, while still considering the 'Built-Up Area' as the most important, clarifies the regions that are likely to be impacted and can help inform regional planning.

The exposure analysis of critical built assets provided further insights beyond land classification and inundation understanding. The refinement of asset exposure at the territorial authority level highlights the localised impact of inundation. Additionally, assessing the exposure of road networks (using ONRC classifications), buildings, bridges, airports, hospitals, and schools helps build a comprehensive understanding of which locations are most susceptible. Notably, Thames-Coromandel District is highly exposed in every asset category considered and as a percentage of asset inventory. Given the character of its topography and road networks, the communities within the Thames-Coromandel District are also susceptible to isolation following natural disasters. Due to its low-lying topography, Napier City faces significant asset exposure during events with small return periods and minimal additional exposure beyond the 1000-year return period.

Auckland has significant asset exposure throughout the territorial authority; however, this remains low as a percentage of the total asset inventory. This is largely explained when looking at the population sizes of the territorial authorities. The median population within each territorial authority is 37,000, whereas Auckland has a population of 1.7 million, which means it has a much larger asset inventory compared to other territorial authorities. Buller District is another interesting case, with a relatively low hazard (in terms of expected tsunami wave amplitude at the shoreline) compared to the rest of New Zealand; however, the resulting inundation makes it one of the most exposed territorial authorities in terms of road length and percentage of the building stock. These infrastructure exposure insights at the territorial authority level enable direct application to the authority decision-making and better enable network redundancy planning. Although the assessment has shown that many major cities around New Zealand are exposed to varying return period tsunami events, it has also proven that many more provincial areas are highly vulnerable to tsunami, reinforcing the necessity for such assessments beyond just the traditional assessments of high-population areas. As Paulik et al. (2020a) emphasise, the variations in exposure highlight that national-scale tsunami mitigation strategies require flexibility, as local approaches are always best when facilitating evacuation preparedness and response plans. Although identification of asset exposure is critical, linking the assets to expected inundation depth and proper fragility

https://doi.org/10.5194/egusphere-2024-3724
Preprint. Discussion started: 11 March 2025

curves will further increase the understanding of asset risk. Williams et al. (2019) review global tsunami impacts on critical infrastructure and produce a semi-quantitative tsunami damage matrix for critical infrastructure components and systems. As Williams et al. (2019) apply the matrix to Christchurch, the matrix can be extended to the entire country.

The exposure modelling results presented in this paper provide valuable insights and introduce a systematic approach to improve the baseline for tsunami assessments. Additionally, it is particularly useful in regions where the density of assets or population does not warrant full hydrodynamic modelling. These types of exposure assessments help identify hot spots of inundation, which can inform localised tsunami preparedness approaches and advise locations for further probabilistic assessments using hydrodynamic modelling or where structural assessments are necessary for critical assets. As discussed, current hydrodynamic modelling is often being implemented in single cities or is implemented at a low resolution and often disregards land cover variations to improve efficiency or enable larger spatial coverage. The ability of the current method to efficiently model inundation while considering a resolution of 10 m by 10 m, alongside land cover variations, enables large-scale assessments at excellent resolution. Therefore, the model enables better large-scale inundation assessments by addressing the limitations of previous approaches, where (1) amplification methods do not account for the multi-dimensional aspects of inundation, (2) attenuation methods are overly simplified, reducing accuracy, and (3) hydrodynamic modelling at large-scales lacks the spatial resolution needed to justify its use or, conversely, cannot be run due to computational or time restrictions at a fine enough resolution.

6 Conclusions

This nationwide tsunami assessment utilises recent probabilistic tsunami hazard data to further understand New Zealand's threat from tsunami events. The modelling method improves on the accuracy of previous inundation modelling methods used in such attempts. Additionally, the efficiency of the model enables the nationwide assessment to be completed with minimal computational cost and time. The consistent approach of this study and the application of the model along the entire coastline of New Zealand is the first of its kind to produce comprehensive nationwide inundation maps for 14 inundation scenarios (7 return periods for the 50th and 84th percentiles) using physics-based modelling at 10 m resolution. These inundation maps have been applied to land cover classification data and infrastructure asset data to better understand the potential exposure of New Zealand to tsunamis across increasing return periods and to help identify the most vulnerable locations. Not only does this method recognise the commonly studied cities as vulnerable (Christchurch, Gisborne and Napier), but it also quantifies their exposure across many assets and land covers. Additionally, this study has identified many provincial areas as hot spots for tsunami inundation and asset exposure that have been overlooked by previous assessments.

The ability of such a model to simulate the entire coastline of New Zealand efficiently supports the implementation of the same methodology internationally with minimal resources (where topography, land use, and hazard data are available). The simple, efficient, yet accurate nature of the model advocates its use in other countries and regions attempting to increase their

https://doi.org/10.5194/egusphere-2024-3724
Preprint. Discussion started: 11 March 2025

tsunami exposure understanding with minimal resource and computational cost. Although PTRA utilising hydrodynamic modelling (with appropriate grid resolution and land cover considerations) is the ideal approach for determining exposure and risk associated with inundation, the current compromises needed to make the modelling efficient and feasible often result in low resolution and disregard for variations in land cover energy dissipation. Therefore, these limitations necessitate an intermediary efficient methodology, which this model effectively provides.

Ongoing tsunami inundation research is required to increase the understanding of tsunami risk, including vulnerability; therefore, this research can be extended by assessing the inundation depths generated by the model to determine the fragility of assets, matching the calculated inundation depths at each asset class to existing fragility and vulnerability asset models. Additionally, the next steps can assess network redundancy in the critical infrastructure networks, including the transportation network, for the different scenarios. The methodology can also be coupled with nationwide flood (and other natural hazard) modelling to generate a complete nationwide "coastal exposure" assessment or combined with seismic and landslide models for near-source events. Alternatively, to improve the inundation findings, the model could be coupled directly with hazard models (with high-resolution shoreline data) to produce inundation outputs for each source scenario, enabling a more comprehensive full probabilistic assessment.

Data availability. Data is available from the authors upon reasonable request

Author contributions. **TK**: Data Curation, Formal Analysis, Writing – Original Draft & Review & Editing. **CW**: Conceptualization, Writing – Review & Editing. **PH**: Conceptualization, Writing – Review & Editing. **LW**: Conceptualization, Writing – Review & Editing, Funding Acquisition

Competing interests. The authors declare no competing interests.

Acknowledgements. The authors would like to acknowledge the Resilience to Nature's Challenges National Science Challenge (grant number CO5X190) as well as the National Hazards Commission Toka Tū Ake for funding and supporting the research.

https://doi.org/10.5194/egusphere-2024-3724
Preprint. Discussion started: 11 March 2025

References

595 Basili, R., Brizuela, B., Herrero, A., Iqbal, S., Lorito, S., Maesano, F. E., Murphy, S., Perfetti, P., Romano, F., Scala, A., Selva, J., Taroni, M., Tiberti, M. M., Thio, H. K., Tonini, R., Volpe, M., Glimsdal, S., Harbitz, C. B., Løvholt, F., & Zaytsev, A. (2021). The Making of the NEAM Tsunami Hazard Model 2018 (NEAMTHM18). Frontiers in Earth Science, 8. https://doi.org/10.3389/feart.2020.616594

Behrens, J., Løvholt, F., Jalayer, F., Lorito, S., Salgado-Gálvez, M. A., Sørensen, M., Abadie, S., Aguirre-Ayerbe, I., Aniel-Quiroga, I., Babeyko, A., Baiguera, M., Basili, R., Belliazzi, S., Grezio, A., Johnson, K., Murphy, S., Paris, R., Rafliana, I., De Risi, R., & Vyhmeister,
600 E. (2021). Probabilistic Tsunami Hazard and Risk Analysis: A Review of Research Gaps. In Frontiers in Earth Science (Vol. 9). Frontiers Media S.A. https://doi.org/10.3389/feart.2021.628772

Berryman, K. (2005). Review of Tsunami Hazard and Risk in New Zealand Review of Tsunami Hazard and Risk in New Zealand Compiled by Kelvin Berryman Prepared for. September.

Burbidge, D., Cummins, P. R., Mleczko, R., & Thio, H. K. (2008). A probabilistic tsunami hazard assessment for Western Australia. Pure
605 and Applied Geophysics, 165(11–12), 2059–2088. https://doi.org/10.1007/s00024-008-0421-x

Dall'Osso, F., Dominey-Howes, D., Moore, C., Summerhayes, S., & Withycombe, G. (2014). The exposure of Sydney (Australia) to earthquake-generated tsunamis, storms and sea level rise: A probabilistic multi-hazard approach. Scientific Reports, 4. https://doi.org/10.1038/srep07401

Davies, G., Griffin, J., Løvholt, F., Glimsdal, S., Harbitz, C., Thio, H. K., Lorito, S., Basili, R., Selva, J., Geist, E., & Baptista, M. A. (2017). A
610 global probabilistic tsunami hazard assessment from earthquake sources. Geological Society, London, Special Publications, 456, 219–244. https://doi.org/10.1144/SP456.5

Downes, G. L., & Stirling, M. W. (2001). Groundwork for development of a probabilistic tsunami hazard model for New Zealand.

Glimsdal, S., Løvholt, F., Harbitz, C. B., Romano, F., Lorito, S., Orefice, S., Brizuela, B., Selva, J., Hoechner, A., Volpe, M., Babeyko, A., Tonini, R., Wronna, M., & Omira, R. (2019). A New Approximate Method for Quantifying Tsunami Maximum Inundation Height
615 Probability. Pure and Applied Geophysics, 176(7), 3227–3246. https://doi.org/10.1007/s00024-019-02091-w

González, J., González, G., Aránguiz, R., Melgar, D., Zamora, N., Shrivastava, M. N., Das, R., Catalán, P. A., & Cienfuegos, R. (2020). A hybrid deterministic and stochastic approach for tsunami hazard assessment in Iquique, Chile. Natural Hazards, 100(1), 231–254. https://doi.org/10.1007/s11069-019-03809-8

Hawker, L., Uhe, P., Luntadila, P., Sosa, J., Savage, J., Sampson, C., & Neal, J. (2022). A 30m global map of elevation with forests and
620 buildings removed. *Environmental Research Letters*, 17. https://doi.org/10.1088/1748-9326/ac4d4f.

FABDEM is produced using Copernicus WorldDEM-30 © DLR e.V. 2010-2014 and © Airbus Defence and Space GmbH 2014-2018 provided under COPERNICUS by the European Union and ESA; all rights reserved. FABDEM is licensed under a Creative Commons 'CC BY-NC-SA 4.0' license. The original license can be found at https://docs.sentinel-hub.com/api/latest/static/files/data/dem/resources/license/License-COPDEM-30.pdf.

625 Hughes, L., Power, W., Lane, E. M., Savage, M. K., Arnold, R., Howell, A., Shaw, B., Fry, B., & Nicol, A. (2023). A novel method to determine probabilistic tsunami hazard using a physics-based synthetic earthquake catalog: A New Zealand case study. *Journal of Geophysical Research: Solid Earth*, 128(12), e2023JB027207. https://doi.org/10.1029/2023JB027207

Horspool, N., Cousins, W. J., & Power, W. L. (2015). Review of Tsunami Risk facing New Zealand: A 2015 Update. In GNS Science.

https://doi.org/10.5194/egusphere-2024-3724
Preprint. Discussion started: 11 March 2025

Horspool, N., Pranantyo, I., Griffin, J., Latief, H., Natawidjaja, D. H., Kongko, W., Cipta, A., Bustaman, B., Anugrah, S. D., & Thio, H. K. (2014). A probabilistic tsunami hazard assessment for Indonesia. Natural Hazards and Earth System Sciences, 14(11), 3105–3122. https://doi.org/10.5194/nhess-14-3105-2014

Imamura, F. (2009). Tsunami modelling: Calculating Inundation and Hazard Maps. In E. N. Bernard & A. R. Robinson (Eds.), *The Sea: Tsunami*. London: Harvard University Press.

Kimpton, T., Higuera, P., Whittaker, C., Wotherspoon, L., & Zorn, C. (2024). A rapid simplified method for determining tsunami inundation extent based on energy conservation. Computer-Aided Civil and Infrastructure Engineering. https://doi.org/10.1111/mice.13168

Leonard, L. J., Rogers, G. C., & Mazzotti, S. (2014). Tsunami hazard assessment of Canada. Natural Hazards, 70(1), 237–274. https://doi.org/10.1007/s11069-013-0809-5

Løvholt, F., Glimsdal, S., Harbitz, C. B., Zamora, N., Nadim, F., Peduzzi, P., Dao, H., & Smebye, H. (2012). Tsunami hazard and exposure on the global scale. In Earth-Science Reviews (Vol. 110, Issues 1–4, pp. 58–73). https://doi.org/10.1016/j.earscirev.2011.10.002

Landcare Research New Zealand. (2018). Land Research Information Systems (LRIS) Portal. Retrieved from https://lris.scinfo.org.nz/layer/104400-lcdb-v50-land-cover-database.

Land Information New Zealand. (2023). Land Information New Zealand (LINZ) Data Service. Retrieved from https://data.linz.govt.nz/. Contains data sourced from the LINZ Data Service licensed for reuse under CC BY 4.0.

Mason, D., & Brabhaharan, P. (2021). The resilience context of transportation routes and recovery after the 2016 Kaikōura earthquake in New Zealand. In WSP (Vol. 54, Issue 2).

NZ Paleotsunami Database (NZPD). (2018). New Zealand Paleotsunami Database. Available at: https://ptdb.niwa.co.nz. [Accessed April 2024].

New Zealand Historical Tsunami Database (NZHTD). (2020). Available at: https://data.gns.cri.nz/tsunami. [Accessed April 2024].

NZ Transport Agency (NZTA). (2013). ONRC - One Network Road Classification. Available at: https://www.nzta.govt.nz/planning-and-investment/planning/road-efficiency-group/transport-insights/data-quality/onrc/.

Paulik, R., Craig, H., & Popovich, B. (2020). A national-scale assessment of population and built-environment exposure in Tsunami evacuation zones. Geosciences (Switzerland), 10(8), 1–15. https://doi.org/10.3390/geosciences10080291

Paulik, R., Stephens, S. A., Bell, R. G., Wadhwa, S., & Popovich, B. (2020). National-Scale Built-Environment Exposure to 100-Year Extreme Sea Levels and Sea-Level Rise. 1–16.

Power, W. (2013). Review of Tsunami Hazard in New Zealand (2013 Update). August.

Power, W. L., Burbidge, D. R., & Gusman, A. R. (2021). The 2021 update to New Zealand's National Tsunami Hazard Model.

Reid, J. A., & Mooney, W. D. (2023). Tsunami Occurrence 1900–2020: A Global Review, with Examples from Indonesia. Pure and Applied Geophysics, 180(5), 1549–1571. https://doi.org/10.1007/s00024-022-03057-1

Rodwell, J., Williams, J. H., & Paulik, R. (2023). Empirical Fragility Assessment of Three-Waters and Railway Infrastructure Damaged by the 2015 Illapel Tsunami, Chile. Journal of Marine Science and Engineering, 11(10). https://doi.org/10.3390/jmse11101991

Roshan, A. D., Basu, P. C., & Jangid, R. S. (2016). Tsunami hazard assessment of Indian coast. Natural Hazards, 82(2), 733–762. https://doi.org/10.1007/s11069-016-2216-1

Sarri, A., Guillas, S., & Dias, F. (2012). Statistical emulation of a tsunami model for sensitivity analysis and uncertainty quantification. https://doi.org/10.5194/nhess-12-2003-2012

Smart, G. M., Crowley, K. H. M., & Lane, E. M. (2015). Estimating tsunami run-up. Natural Hazards, 80(3), 1933–1947. https://doi.org/10.1007/s11069-015-2052-8

https://doi.org/10.5194/egusphere-2024-3724
Preprint. Discussion started: 11 March 2025

Tang, Z., Yang, Y., Melville, B. W., Whittaker, C. N., Shamseldin, A. Y., & Guan, D. (2022). Hydrodynamic Uplift Forces on Submerged Bridge Decks during Bedform Migration. Journal of Hydraulic Engineering, 148(9). https://doi.org/10.1061/(asce)hy.1943-7900.0002005

Williams, J. H., Wilson, T. M., Horspool, N., Lane, E. M., Hughes, M. W., Davies, T., Le, L., & Scheele, F. (2019). Tsunami impact assessment: development of vulnerability matrix for critical infrastructure and application to Christchurch, New Zealand. In Natural Hazards (Vol. 96, Issue 3). https://doi.org/10.1007/s11069-019-03603-6

Williamson, A. L., Rim, D., Adams, L. M., LeVeque, R. J., Melgar, D., & González, F. I. (2020). A Source Clustering Approach for Efficient Inundation modelling and Regional Scale Probabilistic Tsunami Hazard Assessment. Frontiers in Earth Science, 8. https://doi.org/10.3389/feart.2020.591663

Woessner, J., & Farahani, R. J. (2020). Tsunami inundation hazard across Japan. International Journal of Disaster Risk Reduction, 49. https://doi.org/10.1016/j.ijdrr.2020.101654

Xu, Z., Melville, B., Nandasena, N.A.K., Whittaker, C., Shamseldin, A., & Farvizi, F. (2021). Tsunami loads on slab bridges. *Coastal Engineering*, 165, 103853. https://doi.org/10.1016/j.coastaleng.2021.103853

Yoshii, T., Tanaka, S., & Matsuyama, M. (2017). Tsunami deposits in a super-large wave flume. Marine Geology, 391, 98–107. https://doi.org/10.1016/j.margeo.2017.07.020